QUANTIFICATION OF DENDRITIC AND EUTECTIC NUCLEATION UNDERCOOLINGS IN RAPIDLY SOLIDIFIED HYPO-EUTECTIC Al-Cu DROPLETS

A-A. Bogno[1], P. Delshad Khatibi[1], H. Henein[1], Ch-A.Gandin[2]

[1]Department of Chemical and Materials Engineering
University of Alberta
Edmonton, AB T6G 2G6 Canada

[2]MINES ParisTech, Centre de Mise en forme des matériaux,
CNRS UMR 7635, CS10207
06904 Sophia Antipolis
France

Key words: Impulse Atomization, Rapid Solidification, Aluminum-Copper, Undercooling, Microsegregation, Neutron Diffraction, Thermodynamic equilibrium calculations, Coarsening

Abstract

This paper reports on the quantification of primary dendritic and eutectic nucleation undercoolings during rapid solidification of impulse atomized hypo-eutectic Al-Cu droplets. The procedure consists in determining the eutectic fraction of each investigated droplet from the fraction of intermetallic Al_2Cu obtained by Rietveld refinement analysis of neutrons scattering data. The corresponding eutectic nucleation undercooling is then deduced from the metastable phase diagram of the alloy. The dendritic nucleation undercooling is subsequently determined using semi-empirical coarsening models of secondary dendrite arms. The two nucleation undercoolings are finally used as input variables to run a microsegregation model for binary alloys. The fractions of eutectic computed by the microsegregation model compare very favourably with the experimental results.

1. Introduction

Undercooling is observed to various extents in practically every alloy that undergoes solidification processing. Indeed, microstructure development occurs into an undercooled melt after primary phase nucleation. The growth rate depends on the

degree of undercooling [1]. The higher the primary phase nucleation undercooling (ΔT_P), the faster is the growth / solidification rate of the primary phase. Fast dendrite growth induced by a high ΔT_P is, however, accompanied by a large release of latent heat. Therefore, an alloy with a low specific heat will show strong recalescence characterized by a temperature rise which affects the homogeneity of the resulting microstructure and may result in partial re-melting of already solidified dendrites [2]–[4]. Similar undercooling phenomena and recalescence accompany the nucleation of second phases for the formation of the eutectic. This nucleation is termed eutectic undercooling (ΔT_E). ΔT_P and ΔT_E in rapid solidification yield materials with improved mechanical and chemical properties due to the resulting microstructure refinement and reduction of microsegregation [5]. In order to control microsegregation and microstructure distributions in hypoeutectic alloys, it is important to understand how ΔT_P and ΔT_E relate to processing conditions for a specific alloy.

Impulse Atomization (IA) is one of the drop tube types of rapid solidification techniques. With IA, the cooling rate is controlled by the heat exchange between the stagnant gas and the atomized droplets. This heat exchange is a function of upon the nature of the gas in the atomization chamber (helium or nitrogen in the present study), the velocity of the droplets and their size, which depend on atomization operating parameters [6], [7]. Due to practical difficulties, *in-situ* measurements of nucleation temperatures cannot be achieved during IA experiments, consequently a post-mortem method of determining the nucleation temperatures, $T_{P,}$ of the primary phase and T_E of the secondary phases for the formation of eutectic has to be developed. Only in the Electromagnetic Levitation (EML) system, can direct measurements of undercoolings be made. However due to the large size of droplets used in EML (6mm), most of the microstructure of the solidified droplet forms post- recalescence and under conditions of low cooling rate.

The aim of this paper is to consider experimental results obtained by Rietveld refinement analysis of Neutron diffraction (ND) data to determine the eutectic fraction (F_E) and ΔT_E. Then, using ΔT_E in combination with empirical and coarsening models of secondary dendrite arms, ΔT_P will be determined. ΔT_P and ΔT_E will subsequently be used to run a microsegregation model to characterize the microstructures of rapidly solidified droplets generated by IA. Models of equiaxed solidification are rarely compared with microsegregation measurements. Among the few validated models, one

can refer to the work of Gandin *et al*. [8] on solidified droplets during Electro-Magnetic Levitation (EML) and the work on IA droplets published by Prasad et al. [9], [10]and Tourret *et al*. [11]. Tourret's model will be used in the present study. While EML is based on microstructures solidified with relatively low cooling rate ($\dot{T}$) and high ΔT_P, IA is based on relatively high $\dot{T}$ and a high ΔT_P. It is worth mentioning that ΔT_P, a key processing parameter is directly related to microstructural evolution. Therefore, its quantification is an important step in getting access to direct information on the specific solidification path and thermal history controlling microstructures development. Thus, analysis of IA droplets will allow us to map out a wide range of solidification microstructures so that their processing history can be inferred from the knowledge of ΔT_P and $\dot{T}$.

2. Experimental

Rapidly solidified Al-Cu droplets of different sizes were generated by IA under nitrogen and under helium atmospheres [9]. A schematic representation of the IA experimental setup is given in Fig.1. A summary of the investigated samples and the experimental conditions are given in Table I. The droplets considered in the present investigation were atomized from a melt temperature of 1123 K (850°C) in an oxygen-free chamber (less than 20 ppm oxygen [10]) filled with either nitrogen or helium. After atomization, the droplets were washed, dried and sieved into different size ranges varying from (180µm - 212 µm) to (850µm -1000µm). In the present study, for each size range, an average value is considered.

3. Results

3.1. Eutectic fraction F_E and eutectic nucleation undercooling ΔT_E

3.1.1. Procedures for estimating F_E and ΔT_E

In a published work by Prasad et al [9], F_E for the droplets under investigation were obtained using a combination of measured values by Stereology and Neutron Diffraction (St.+ND). And, the corresponding ΔT_E were estimated based on interpolations of experimental measurements on Al-Cu droplets reported by Gandin *et al* [8]. In this section, a metastable phase diagram of the Al-Cu system will be used in combination with Gulliver-Scheil (GS) model of microsegregation and Neutron

Diffraction (ND) data to estimate F_E and the corresponding ΔT_E. Indeed, considering that rapid solidification resulting from high cooling rate does not promote time dependent processes such as diffusion. Therefore, the GS model of microsegregation (a model that assumes no diffusion in the solid and complete mixing in the liquid) is considered to be more suitable for the determination of eutectic fractions in rapidly solidified droplets. If the nucleation of eutectic structure phases occurred without any undercooling, i.e. at the eutectic temperature of each alloy, GS model predicts F_E (in wt.) to be 46% for Al-17wt% Cu, 25% for Al-10wt% Cu and 12% for Al-5wt% Cu. These values are all higher than the equilibrium eutectic fractions (EQ) calculated by the Lever Rule (LR) (Table I). However, the eutectic structure phases in rapidly solidified droplets are not likely to nucleate at the equilibrium eutectic temperature considering the undercooling of droplets. Since *in-situ* measurements of nucleation temperatures cannot be achieved during IA experiments, a post-mortem procedure to determine ΔT_E needs to be developed. It must combine experimental results of phase fractions obtained from ND data and the extensions of solidus and liquidus lines of the equilibrium phase diagram of the investigated alloys following the steps described below:

(i) The weight fractions of eutectic are calculated at various temperatures below equilibrium eutectic temperature using the GS microsegregation equation (1).

$$F_E(T) = \left(\frac{C_E(T)}{C_0}\right)^{\frac{1}{k(T)-1}} \quad (1)$$

It is assumed that no re-melting takes place after eutectic nucleation. Thermodynamic calculations of phases are carried out by extending the solidus and liquidus lines in the aluminum rich hypoeutectic region of the Al-Cu phase diagram (Fig.2) [*Thermo-Calc Database, TCBIN Version1.1, 2008*]. Thus, the temperature *T* could be varied from the equilibrium eutectic temperature T_E = 821 K (548°C) to 790 K (517°C), the temperature corresponding to the new maximum solute solubility obtained after extending the solidus and liquidus lines (through suspension of θ-Al_2Cu phase). $C_E(T)$ is the temperature dependent liquid composition varying from the equilibrium eutectic composition (33wt% Cu) to the maximum solubility limit in the liquid (38.7 wt%). C_0

is the nominal composition of the alloy under consideration (5, 10 or 17wt% Cu) and k is the temperature dependent partition coefficient.

(ii) The weight fraction of θ-Al_2Cu phase $F_\theta(T)$ at each temperature below T_E is calculated from the eutectic weight fraction using Eq.2.

$$F_\theta(T) = F_{\theta E} \times F_E(T) \quad (2)$$

$F_{\theta E}$ is the fraction of θ-Al_2Cu in the eutectic structure, it is assumed that the nucleation of θ-Al_2Cu is followed by a temperature rise due to recalescence (latent heat released greater than the convective heat loss through the droplet) up to T_E and that most of the θ-Al_2Cu forms at the equilibrium eutectic temperature after recalescence as previously shown by modelling results reported in [4]. Consequently, $F_{\theta E}$ could be determined by the LR at the equilibrium eutectic temperature.

(iii) $F_\theta(T)$ is calculated at various temperatures (Eq.2) and compared with the experimental fraction of θ-Al_2Cu determined by Rietveld refinement analysis of ND data. Consequently, the actual weight fraction of eutectic, $F_E(T)$, is determined as the value corresponding to $F_\theta(T)$ that matches the experimental fraction of θ-Al_2Cu. A temperature T_E' *(*corresponding to that liquid temperature T when $F_\theta(T)$ matches the experimental weight fraction of θ-Al_2Cu) could therefore be defined as the eutectic nucleation temperature so that ΔT_E can be defined as the temperature difference between the equilibrium eutectic temperature T_E and the temperature T_E' at which the actual eutectic nucleation occurred (Equation 3).

$$\Delta T_E = T_E - T_E' \quad (3)$$

3.1.2. Variations of F_E with alloy composition

Fig. 3 shows the variation of weight percent eutectic with alloy nominal composition and also compares the eutectic fractions obtained through the metastable extensions of solidus and liquidus lines (F_E) with corresponding results obtained by combination of stereology and neutron diffraction ($F_E\_St + ND$). The GS predictions and the

equilibrium solidification (EQ) calculated by the LR are also plotted. It can be observed that:

(i) F_E is in good agreement with $F_E\_St + ND$ for all of the investigated droplets.

(ii) F_E increases with Cu-content (alloy nominal composition) as expected from the simple EQ and GS approximations.

(iii) For Al-Cu alloys of composition 5wt% and 10wt% Cu, F_E lies between predicted values by EQ and GS predictions.

(iv) F_E for Al-17wt% Cu lies below predictions by EQ and GS.

Indeed, during rapid solidification, a delay in the nucleation of θ-Al_2Cu phase of the eutectic structure is possible so that the dendritic phase is allowed to solidify below the equilibrium eutectic nucleation temperature [8], [9]. Consequently, there will be a smaller amount of liquid left when eutectic reaction takes place. Hence, lower experimental eutectic fractions are obtained as compared to GS and EQ predictions.

Table II shows a summary of the experimental results obtained by stereology and neutron diffraction that lead to the estimation of eutectic fractions.

3.1.3. Variations of F_E with ΔT_E

Fig. 4 shows the variation of weight percent eutectic with eutectic nucleation undercooling. For each alloy composition F_E is shown to be slightly decreasing with ΔT_E. The higher the nominal composition of the alloy the more this decrease is observed. As already mentioned above, below the equilibrium eutectic temperature, primary dendrites can continue to grow so that there is less liquid available when eutectic reaction takes place at a lower temperature, hence the slight decrease of weight percent eutectic as eutectic undercooling is increased. This result is in agreement with previously reported results by Prasad et al. [9], [10]

3.2. Determination of primary dendritic nucleation undercooling ΔT_P

3.2.1. Procedures for estimating ΔT_P

Definition and assumptions

Primary dendritic nucleation undercooling ΔT_P is defined as the difference between the equilibrium liquidus temperature T_L and the nucleation temperature T_P of the primary dendritic α -phase. To determine ΔT_P it is assumed that:

(i) The α-phase forms as a result of nucleation, growth and coarsening up to the nucleation of the eutectic. Following the nucleation of θ-Al_2Cu phase, no primary solid formation takes place. This assumes that the eutectic structure grows as a front in between the dendrites as shown in [12], [13] using in-situ radiography imaging of directional solidification of Al-30wt%Cu. During eutectic growth, no liquid is in contact with the primary α -phase.

(ii) There is no primary α-phase re-melting due its recalescence.

(iii) Most of the dendrites that have formed did so during coarsening so that a semi-empirical relationships such as the one reported by Kurz and Fisher [14] can be used to describe the secondary dendrite arms spacing λ_2 as a function of solidification time (Eq.4a).

$$\lambda_2 = 5.5(Mt_{SL})^{1/3} \tag{4}$$

where t_{SL} is the local solidification time and M includes all temperature dependent terms. Taking the dendrite coarsening results of Kattamis [15], Roosz and co-workers [16] have defined the coarsening parameter M as:

$$M = \frac{\gamma D_L(T)T}{m(1-k)\Delta H C_L} \tag{5}$$

where γ is the energy of solid/liquid interface, ΔH is the latent heat of solidification, m is the liquidus slope, k is the solute partition coefficient, D_L is the solute diffusion coefficient in liquid phase and C_L is the solute composition in liquid phase.

The coarsening parameter M as expressed in Eq.4b is found to decrease with decreasing temperature during solidification (Fig.5) so that a mean value of $\bar{M}$ can be calculated according to Eq.5 as the average value of M varying from the nucleation temperature of primary α-phase T_P to the eutectic nucleation temperature T'_E .

$$\bar{M} = \frac{1}{T_P - T'_E}\int_{T'_E}^{T_P} M(T)dT \tag{6}$$

Eq.4a can therefore be written as:

$$\lambda_2 = 5.5(\bar{M} t_{SL})^{1/3} \quad (7)$$

Combination of experimental results and empirical models

Secondary dendrite arm spacing (SDAS) λ_2 is shown to be related to the average solidification cooling rate ($\dot{T} = \frac{\Delta T_{SL}}{t_{SL}}$) by a power law described by Eq.7 [17], [18].

$$\lambda_2 = A\,(\dot{T})^{-n} \quad (8)$$

ΔT_{SL} is the local solidification interval, *A* and *n* are alloy-dependent parameters obtained from the best fitting curves (R^2>0.90) of λ_2 *Vs* $\dot{T}$. The values of $\dot{T}$ and λ_2 used to estimate *A* and *n* for the investigated samples (Table I) are the ones reported in [9]. The parameter *A*, described as a "composition-sensitive" coefficient by Eskin et al [17] is found to be decreasing with increasing nominal alloy composition C_0 (*A* is equal to 43. 96, 22.66 and 20.92 respectively as C_0 varies from 5wt%, 10wt% and 17wt%) while coefficient *n* is less sensitive to the alloy composition ($n \simeq 1/3$ for the three investigated alloys). Thus, for each investigated droplet, $\bar{M}$ and *A* can be determined by equating Eq.7 and Eq.8. (Substituting $\frac{\Delta T_{SL}}{t_{SL}}$ for $\dot{T}$).

$$A = 5.5(\bar{M} \Delta T_{SL})^{1/3} \quad (9)$$

Knowing the experimental value of *A* for each alloy composition, $\bar{M}$ and ΔT_{SL} ($= T_P - T'_E$) were varied from $T_P = T_L$ to $T_P = T'_E$ until the experimental value of *A* is obtained. Then ΔT_P is deduced (Eq.10) from the corresponding T_P.

$$\Delta T_P = T_L - T_P \quad (9)$$

3.2.2. Variations of ΔT_P with average droplets size

Primary nucleation undercooling is plotted as a function of average droplets size. Fig.6 shows that there is little to no variation of the ΔT_P within the investigated range of droplet sizes (180µm-1000µm) for the three investigated Al-Cu compositions under both He and N_2. Therefore, it can be said that primary dendritic nucleation undercooling and heat extraction rate are not correlated in the case observed. This is in agreement

with EML experiments where high dendritic nucleation undercooling can be obtained followed by low solidification cooling rate [19]. Indeed, undercooling depends not only on the nucleation mode, but also on other factors such as the size and nature of nuclei as well as the thermo-physical properties of the melt [20] [21]. It is worth noting that Al-5wt% Cu droplets display ΔT_P ~14K , a value that is very close to 15K obtained for the same droplets in [9] by trial and error using solid fraction around the nucleation point on droplets microstructures revealed by micro-tomography images.

Table IV summarizes the experimental results of F_E , ΔT_E and ΔT_P for each investigated alloy with respect to cooling gas and droplet size . ΔT_P values obtained with the methodology presented in this paper will be used as input variables to run the microsegregation model so that the output results will be compared with the experimental results used in this methodology.

3.3. Microsegregation model

3.3.1. Brief description

A microsegregation model has been developed by Tourret et al. [22], [23]. It is an extension of the equiaxed solidification model developed successively by [8], [9], [24–28] and coupled with Thermo-Calc. The model is applicable to an atomized (spherical) droplet under a non-moving gas. It is limited to binary alloys with uniform and constant density in all phases and the growth of the structures is isotropic during the entire solidification process. It is also assumed that solidification is controlled by solute diffusion in both solid and liquid and the temperature is homogeneous within the droplet.

The input variables of the model consist of: (*i*) the melt temperature, (*ii*) the droplet size (iii) the gas type and properties, (iv) the alloy composition and properties, (v) the alloy phase diagram, (vi) the solute diffusion coefficients, (vii) the secondary dendrite arm spacing, (viii) the Gibbs-Thompson coefficients, (ix) the contact angles between phases and (x) the primary dendritic and secondary eutectic nucleation undercoolings. A single nucleation event at a given temperature is assumed for nucleation.

The model's output gives the thermal history of the solidified droplet (cooling rate, enthalpy, variation of phases, recalescence, etc.) and predicts microsegregation within the droplet during solidification in terms of weight percent eutectic F_E *(model).*

3.3.2. Model prediction of eutectic fraction

ΔT_P and ΔT_E obtained for each investigated droplet are used as input variables to run the model. F_E *(model)* for each investigated droplet is plotted as a function of composition (Fig.7a). The conclusions given for the experimental results in section 3.1.2 are found to apply very well for the model predictions. Then, the F_E *(model)* are compared with the experimental values, Fig.7b shows that these values are in good agreement with the experimental results. Note that the microsegregation model predicts that only 0.2 to 23 % of the total solidification time account for primary α-phase nucleation and recalescence. Thus most of the primary dendrites are formed during coarsening. Hence the use of a coarsening model to estimate the dendritic nucleation undercooling is justified.

3.3.3. Model prediction of primary dendritic solid fraction during recalescence

Recalescence occurs when the rate of heat generation during phase transformation is higher than the rate of heat loss by the droplet to the surrounding gas. It is characterized by a rise of temperature after nucleation. During rapid solidification by IA, if a phase formation happened at a rate sufficiently fast relative to the time required for heat exchange with surrounding gas, an overall adiabatic condition could be established between a droplet and the stagnant surrounding gas.

Fig.8 shows the variation of the primary solid fraction F_R formed during recalescence with ΔT_P for the three investigated alloys. As expected, F_R is a linear function of ΔT_P.

Assuming that during the period of recalescence the solidification occurs under adiabatic conditions, the primary dendritic solid fraction F_R formed during recalescence (therefore adiabatically) can be determined using equation (11).

$$F_R = \left(\frac{C_p^l}{\Delta H_f}\right)\Delta T_P \qquad (10)$$

Where C_p^l is the melt heat capacity, ΔH_f the latent heat of fusion and ΔT_P the primary α-phase nucleation undercooling.

The characteristic undercooling or hypercooling limit ΔT_{hyp} of the melt is given by

$$\Delta T_{hyp} = \frac{\Delta H_f}{C_p^l} \quad (11)$$

Consequently the adiabatic primary dendritic solid fraction is given by

$$F_R = \frac{\Delta T_P}{\Delta T_{hyp}} \quad (12)$$

ΔT_P can therefore be defined as a fraction (F_R) of the hypercooling limit of each alloy, ΔT_{hyp} of the investigated alloys are given in Table II. Thus, using Equation 13 and the values of F_R predicted by the microsegregation model, the corresponding ΔT_P for each investigated droplet can be back calculated.

Fig.9 shows a plot of ΔT_P *(theory)* calculated using Eq.13 against the ΔT_P *(exp)* estimated by the coarsening model for each investigated alloy. The points almost overlapping the *X=Y* curve is a clear indication that within the limit of experimental measurements ΔT_P (exp) are in agreement with the theoretical values. Therefore, the experimental methodology used to determine ΔT_P is justified.

3.3.4. Effect of primary dendritic nucleation undercooling on recalescence

Fig.10 shows the variation with ΔT_P of the characteristic temperatures during the alloys solidification. It can be observed that for all the investigated alloys, the recalescence temperature T_R (maximum temperature reached by the melt subsequent to recalescence) rises just below the liquidus temperature. This result indicates that there is no remelting taking place after primary dendritic phase nucleation. As expected, the temperature increase during recalescence is a function of ΔT_P.

3.3.5. Effect of primary dendritic nucleation undercooling on eutectic fraction

The microsegregation model is run with the dendritic nucleation undercooling being equal to zero but the eutectic nucleation undercooling is kept as experimentally estimated. Fig.11 shows a comparison of the model outputs of weight percent eutectic taking into account the dendritic undercooling (E1) and ignoring the dendritic nucleation undercooling (E2). It can be seen that all the points lie on the X=Y curve, indicating that the predicted weight percent eutectic is the same with or without the primary dendritic nucleation undercooling. Therefore, it can be concluded that the primary dendritic undercooling does not influence the fraction of eutectic structure.

4. Conclusions

Rapid solidification of impulse atomized Al-Cu droplets of compositions 5, 10 and 17 wt% Cu, classified in different size ranges, were analysed. The solidus and liquidus lines of the hypoeutectic side of Al-Cu system were extended by Thermo-Calc to account for metastability resulting from rapid solidification and high nucleation undercoolings. Experimentally measured phase fractions by rietveld refinement of neutron diffraction (ND) data were used to estimate the weight percent eutectic in each droplet and the corresponding eutectic nucleation undercooling from the phase diagram. A very good agreement was found between the estimated weight percent eutectic and the published results obtained by combining stereology measurements and ND data. Dendritic nucleation undercooling was then calculated by combining semi-empirical models of SDAS with the estimated eutectic nucleation undercooling. The dendritic and eutectic nucleation undercoolings were then used as input variables to run a validated microsegregation model. The output results were found to be in agreement with the theory of a spherical droplet solidifying in a quiescent gas.

Acknowledgements

The authors are grateful to the Natural Sciences and Engineering Research Council of Canada (NSERC), Novelis, the Canadian Space Agency (CSA), the European Space Agency (ESA) and the Agence Nationale de Recherche (ANR-France) under MIMOSA for their financial support. Drs. M.Rappaz and Jonas Valloton are also acknowledged for fruitful discussions.

References

[1] J. Lipton, M. E. Glicksman, and W. Kurz, "Dendritic growth into undercooled alloy metals," *Materials Science and Engineering*, vol. 65, no. 1. pp. 57–63, 1984.

[2] R. Heringer, C.-A. Gandin, G. Lesoult, and H. Henein, "Atomized droplet solidification as an equiaxed growth model," *Acta Mater.*, vol. 54, no. 17, pp. 4427–4440, Oct. 2006.

[3] J. Chen, U. Dahlborg, C. M. Bao, M. Calvo-Dahlborg, and H. Henein, "Microstructure evolution of atomized Al-0.61 wt pct Fe and Al-1.90 wt pct Fe alloys," *Metall. Mater. Trans. B Process Metall. Mater. Process. Sci.*, vol. 42, no. 3, pp. 557–567, 2011.

[4] C.-A. G. S. Mosbah, M. Bellet, "No Title," *Metall.Mater.Trans*, vol. 41, pp. 651–669, 2010.

[5] M. C. Flemings, "Solidification processing," *Metall. Trans.*, vol. 5, no. 10, pp. 2121–2134, 1974.

[6] H. Henein, "Single fluid atomization through the application of impulses to a melt," *Mater. Sci. Eng. A*, vol. 326, no. 1, pp. 92–100, Mar. 2002.

[7] J. B. Wiskel, K. Navel, H. Henein, and E. Maire, "Solidification study of aluminum alloys using Impulse Atomization: Part II. Effect of cooling rate on microstructure," in *Canadian Metallurgical Quarterly*, 2002, vol. 41, no. 2, pp. 193–204.

[8] C.-A. Gandin, S. Mosbah, T. Volkmann, and D. M. Herlach, "Experimental and numerical modeling of equiaxed solidification in metallic alloys," *Acta Mater.*, vol. 56, no. 13, pp. 3023–3035, Aug. 2008.

[9] A. Prasad, S. Mosbah, H. Henein, and C.-A. Gandin, "A Solidification Model for Atomization," *ISIJ International*, vol. 49, no. 7. pp. 992–999, 2009.

[10] A. Prasad, "No Title," 2006.

[11] D. Tourret, G. Reinhart, C.-A. Gandin, G. N. Iles, U. Dahlborg, M. Calvo-Dahlborg, and C. M. Bao, "Gas atomization of Al–Ni powders: Solidification modeling and neutron diffraction analysis," *Acta Mater.*, vol. 59, no. 17, pp. 6658–6669, Oct. 2011.

[12] D. Ruvalcaba, R. H. Mathiesen, D. G. Eskin, L. Arnberg, and L. Katgerman, "In-Situ analysis of coarsening during directional solidification experiments in high-solute aluminum alloys," *Metall. Mater. Trans. B Process Metall. Mater. Process. Sci.*, vol. 40, no. 3, pp. 312–316, 2009.

[13] R.Mathiesen and L.Anberg, "No Title," *Acta Mater*, vol. 53, pp. 947–956, 2005.

[14] W.Kurz and D.J.Fisher, *Fundamentals of Solidification*, 4th editio. CRC Press, 1998.

[15] J. C. C. and M. C. F. T. Z. KATTAMIS, "No Title," *Trans.AIME*, vol. 239, p. 1504, 1967.

[16] H. E. Roosz, A.Halder, E.Exner, "Numerical calculation of microsegregation in coarsened dendritic microstructures," *Mater. Sci. Technol. 2013*, vol. 2, pp. 1149–1155, 1986.

[17] D. Eskin, Q. Du, D. Ruvalcaba, and L. Katgerman, "Experimental study of structure formation in binary Al-Cu alloys at different cooling rates," *Mater. Sci. Eng. A*, vol. 405, no. 1–2, pp. 1–10, 2005.

[18] R. F. C. and N. J. A. A.M.Mullis, L.Farrell, “No Title,” *Met. Mater. Trans.B*, vol. 44 (4), pp. 1073–5615, 2013.
[19] G. P. G. E.Schleip, R. Willnecker, D.M. Herlach, “No Title,” *Mater.Sci.Eng*, vol. 98, pp. 39–42, 1988.
[20] T. E. Quested and A. L. Greer, “The effect of the size distribution of inoculant particles on as-cast grain size in aluminium alloys,” *Acta Mater.*, vol. 52, no. 13, pp. 3859–3868, 2004.
[21] T. E. Quested and A. L. Greer, “Grain refinement of Al alloys: Mechanisms determining as-cast grain size in directional solidification,” *Acta Mater.*, vol. 53, no. 17, pp. 4643–4653, 2005.
[22] D. Tourret and C.-A. Gandin, “A generalized segregation model for concurrent dendritic, peritectic and eutectic solidification,” *Acta Mater.*, vol. 57, no. 7, pp. 2066–2079, Apr. 2009.
[23] D. Tourret, C.-A. Gandin, T. Volkmann, and D. M. Herlach, “Multiple non-equilibrium phase transformations: Modeling versus electro-magnetic levitation experiment,” *Acta Mater.*, vol. 59, no. 11, pp. 4665–4677, Jun. 2011.
[24] M. Rappaz and P. Thévoz, “Solute diffusion model for equiaxed dendritic growth,” *Acta Metall.*, vol. 35, no. 7, pp. 1487–1497, Jul. 1987.
[25] M. Rappaz and P. H. Thévoz, “Solute diffusion model for equiaxed dendritic growth: Analytical solution,” *Acta Metall.*, vol. 35, no. 12, pp. 2929–2933, Dec. 1987.
[26] C. Y. Wang and C. Beckermann, “A multiphase solute diffusion model for dendritic alloy solidification,” *Metall. Trans. A*, vol. 24, no. 12, pp. 2787–2802, 1993.
[27] C. Y. Wang and C. Beckermann, “A unified solute diffusion model for columnar and equiaxed dendritic alloy solidification,” *Materials Science and Engineering: A*, vol. 171, no. 1–2. pp. 199–211, 1993.
[28] M.A Martorano et al, “No Title,” *Metall.Mater.Trans.A*, vol. 34A, pp. 1657–1674, 2003.

List of figures

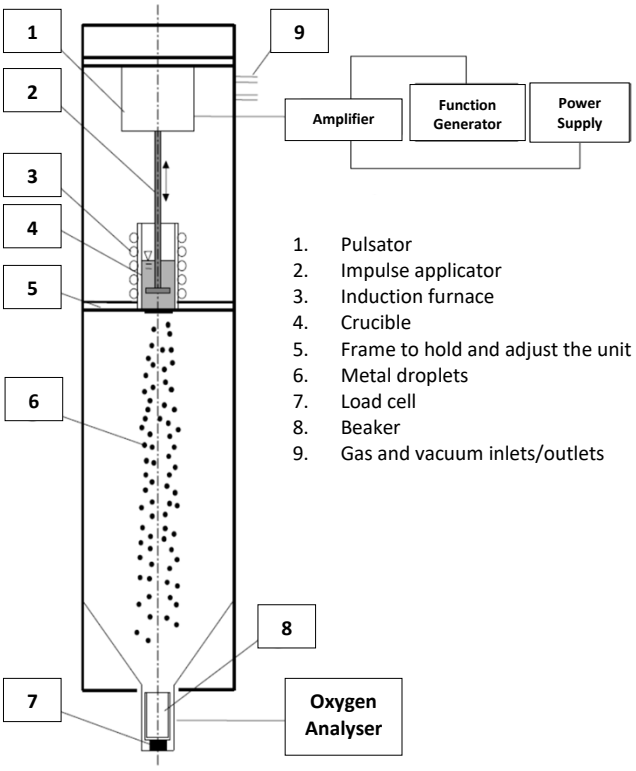

Fig. 1: Schematic of the Impulse Atomization (IA) setup

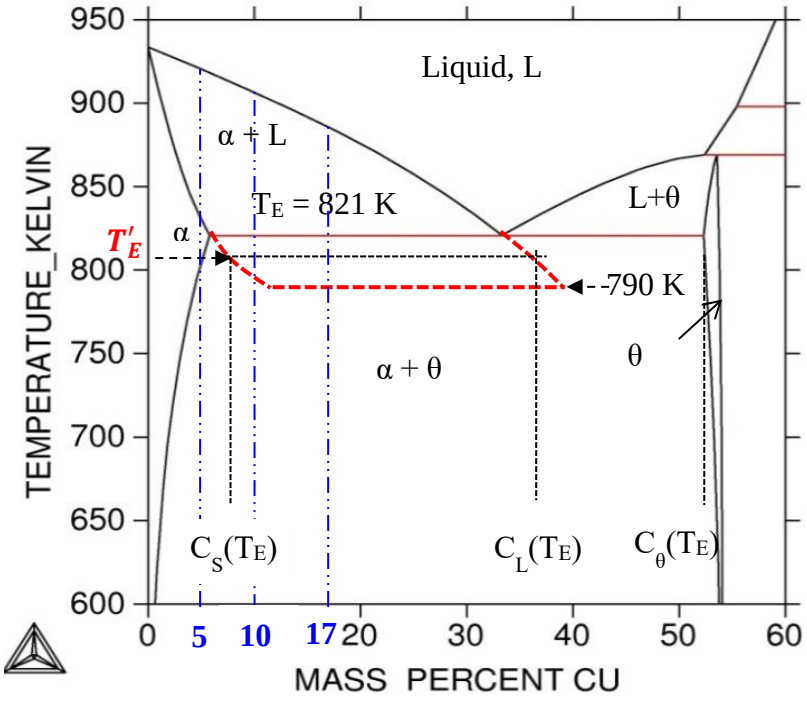

Fig.2: Aluminum rich hypoeutectic region of Al-Cu phase diagram calculated by Thermo-Calc. Extension of solidus and liquidus lines obtained by suspension of θ-Al_2Cu as well as the investigated alloy compositions are indicated by dashed lines.

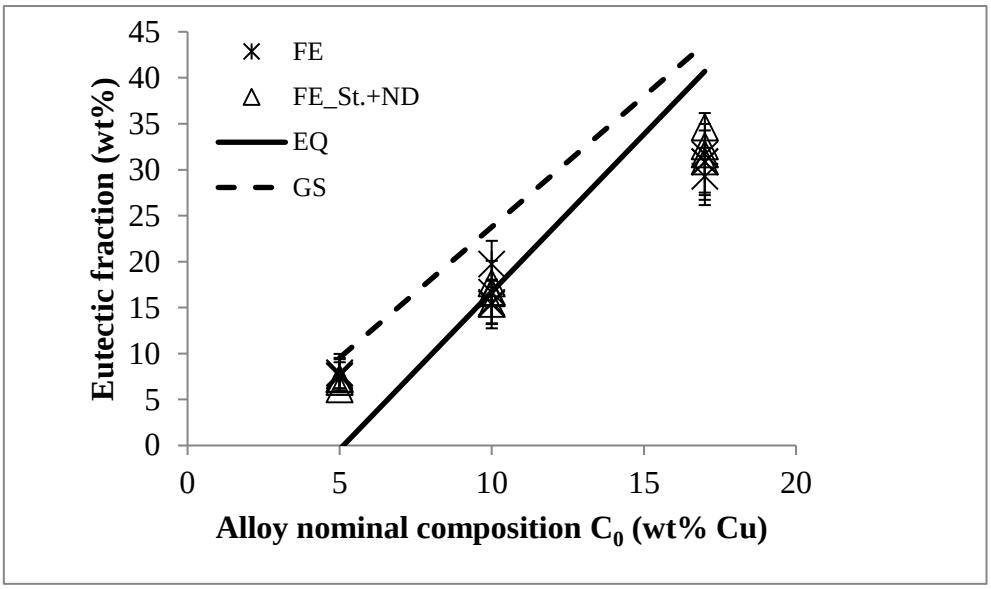

Fig. 3: Comparison of weight percent eutectic obtained from the metastable phase diagram with results from combination of Stereology (St.) and Neutron Diffraction (ND) data, predictions by Scheil-Gulliver-Scheil (GS) and the Lever Rule (LR).

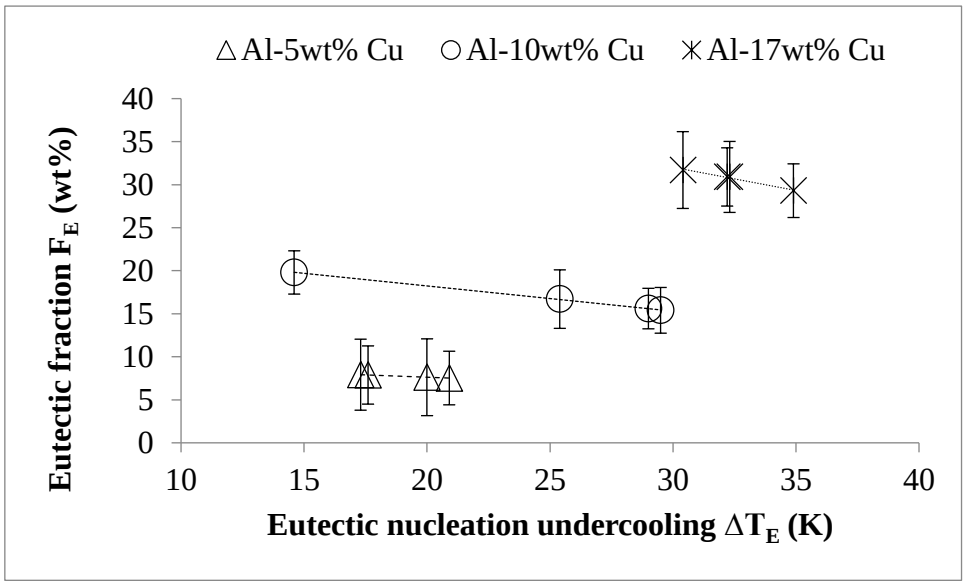

<u>Fig.4:</u> Variation of weight percent eutectic with eutectic nucleation undercooling

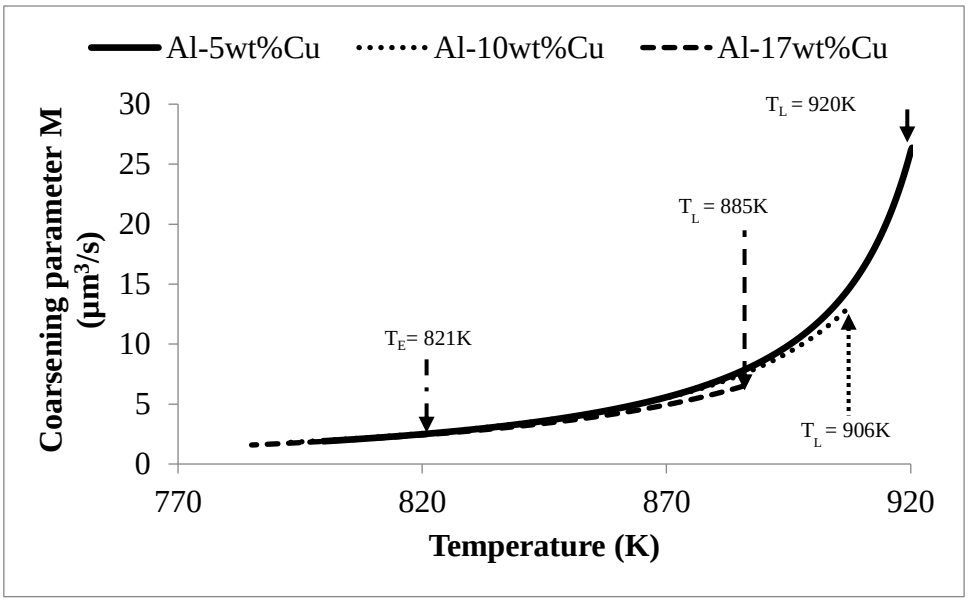

Fig.5: Variation from T_L to T'_E of coarsening parameters of Al-Cu droplets atomized under He. Droplets size: 196 μm

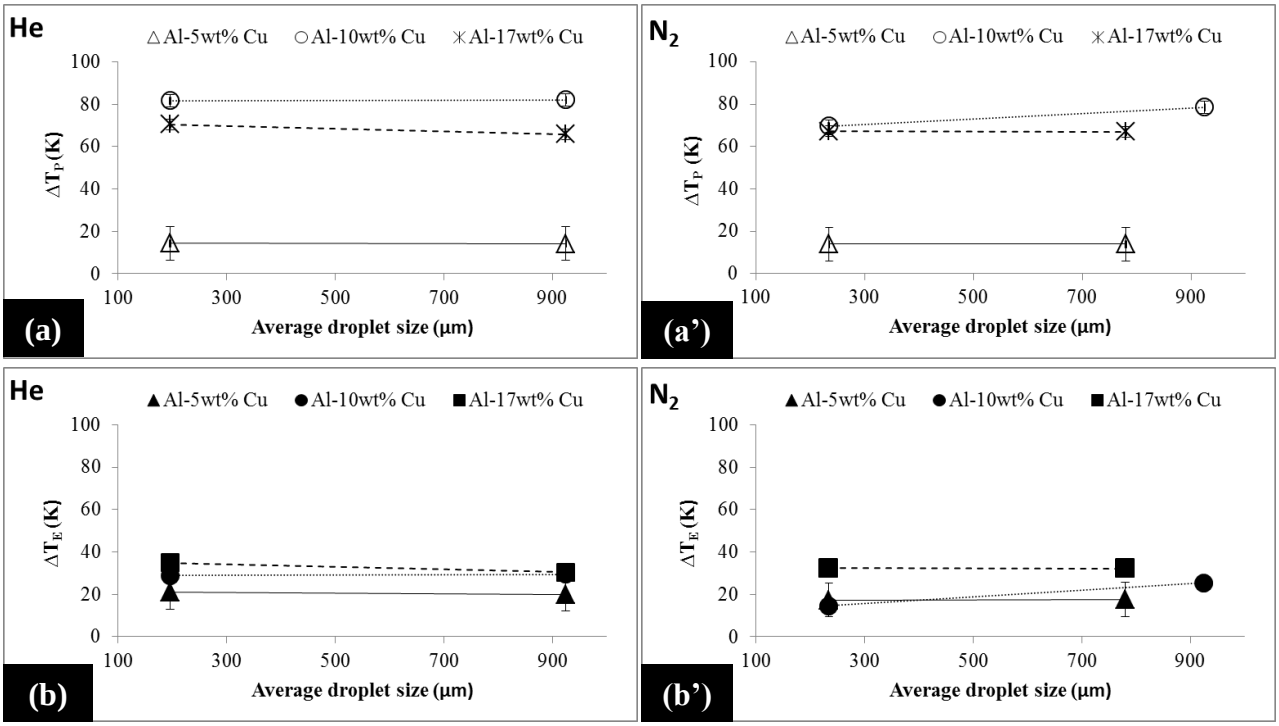

Fig.6: Variation of dendritic and eutectic nucleation undercooling with average droplet size for the three investigated alloys atomized under He and N_2.

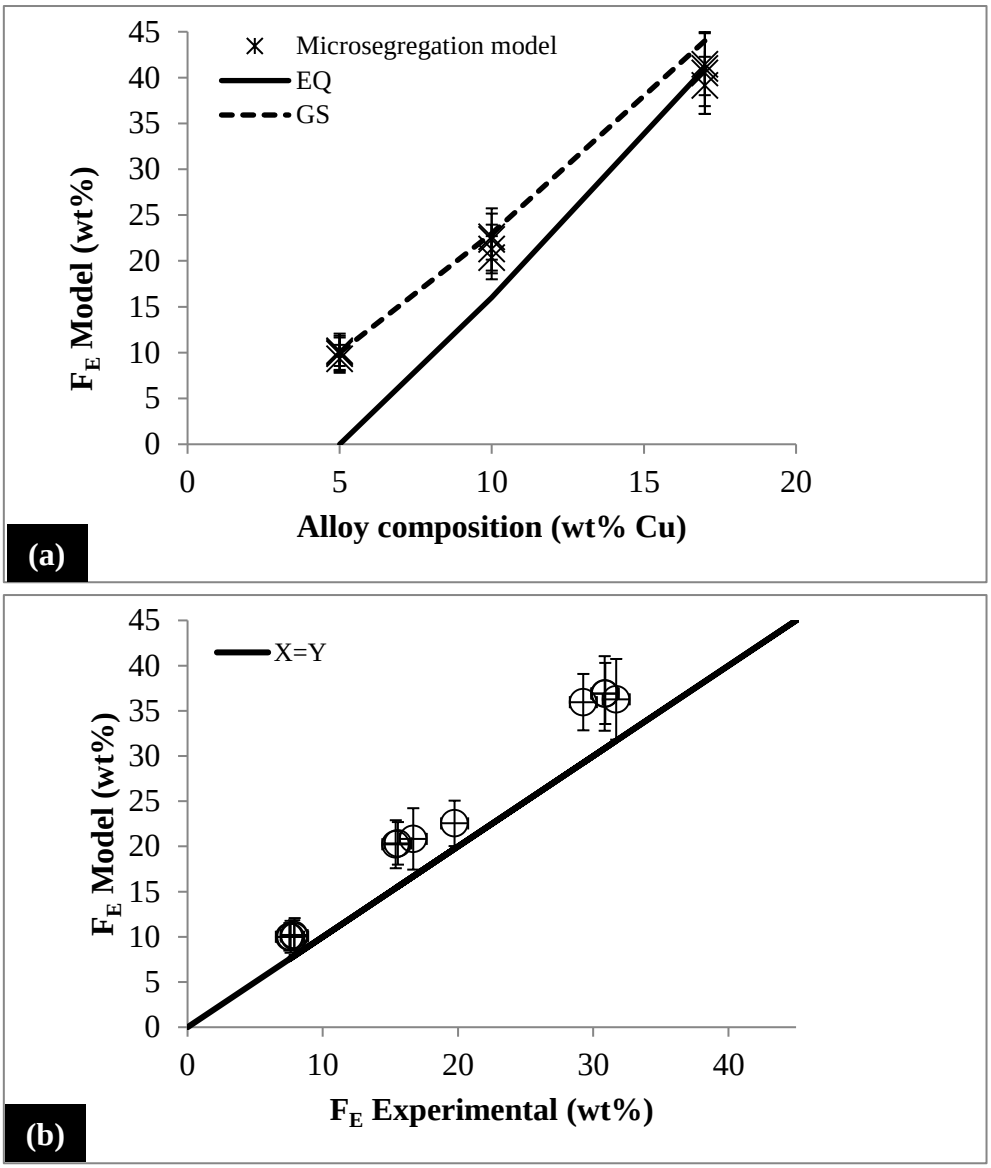

Fig.7: (a) Model output of weight percent eutectic as a function of alloys composition and comparison with Gulliver-Scheil (GS) and the Lever Rule (LR) (b) Comparison of experimental results with models output results of weight percent eutectic for the investigated droplets.

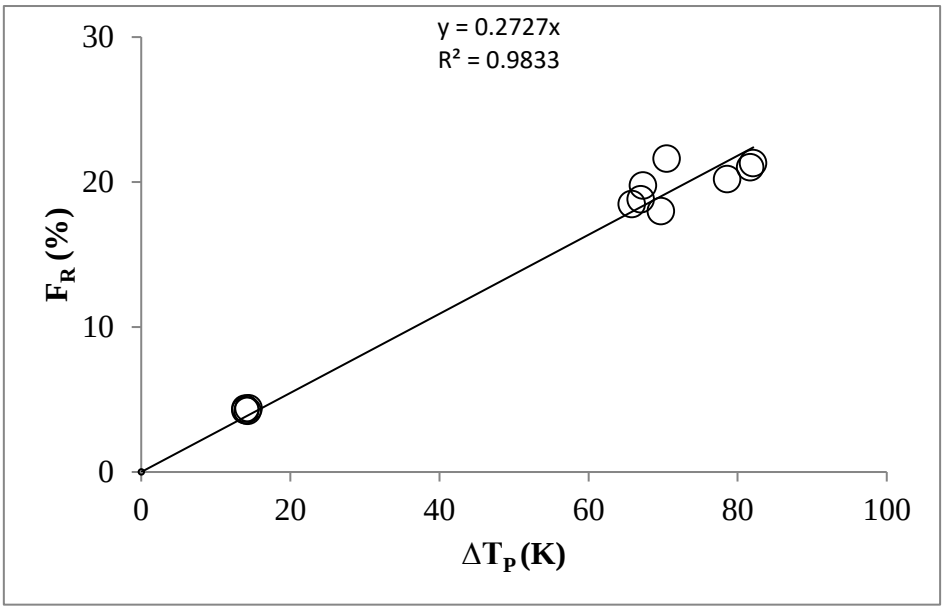

Fig.8: Primary solid fraction F_R formed during recalescence as a function of the primary dendritic nucleation undercooling ΔT_P for the three investigated alloys.The data are fitted with a linear curve.

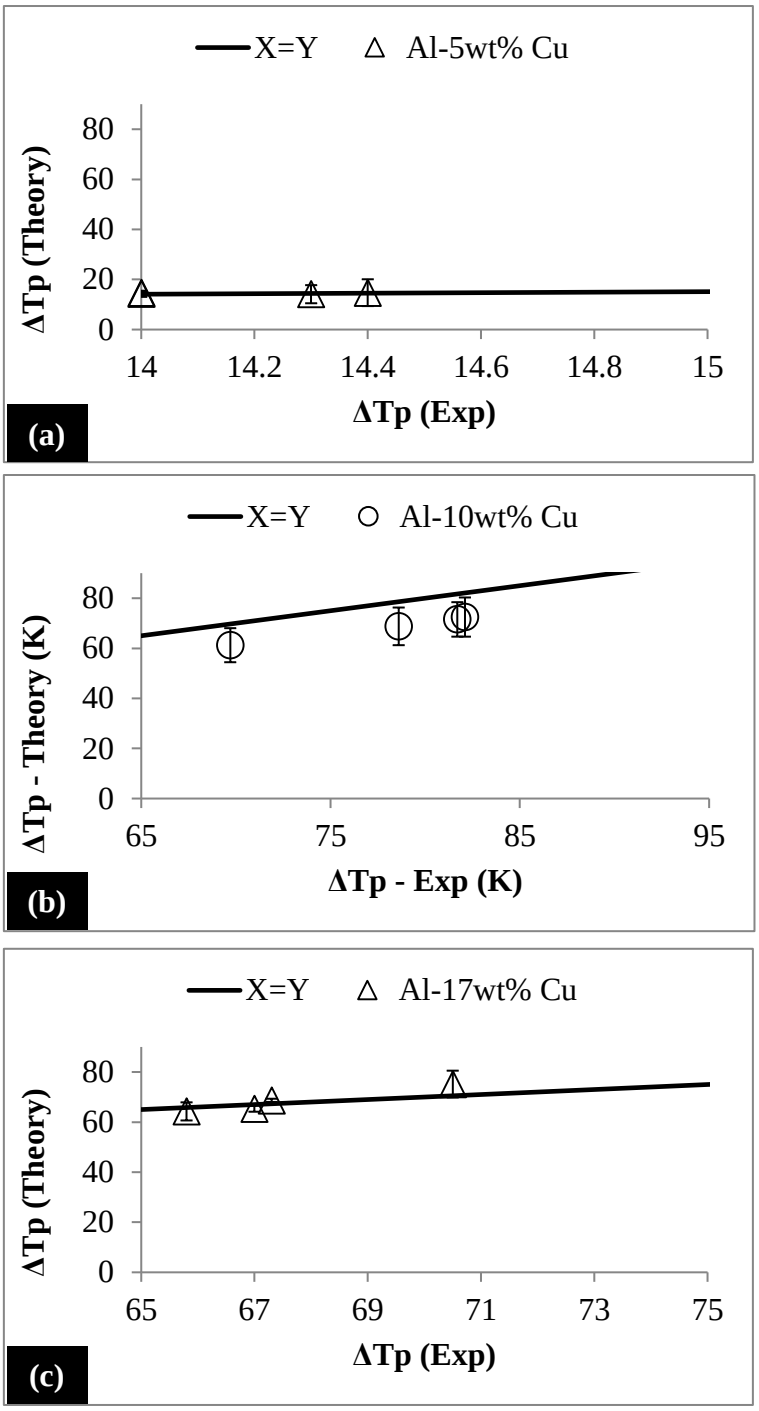

<u>Fig.9</u>: Theoretical p*rimary dendritic nucleation undercooling* ΔT_P (theory) *calculated using the definition of hypercooling limit as a function of* ΔT_P (exp) *estimated by the coarsening model for each investigated alloy.*

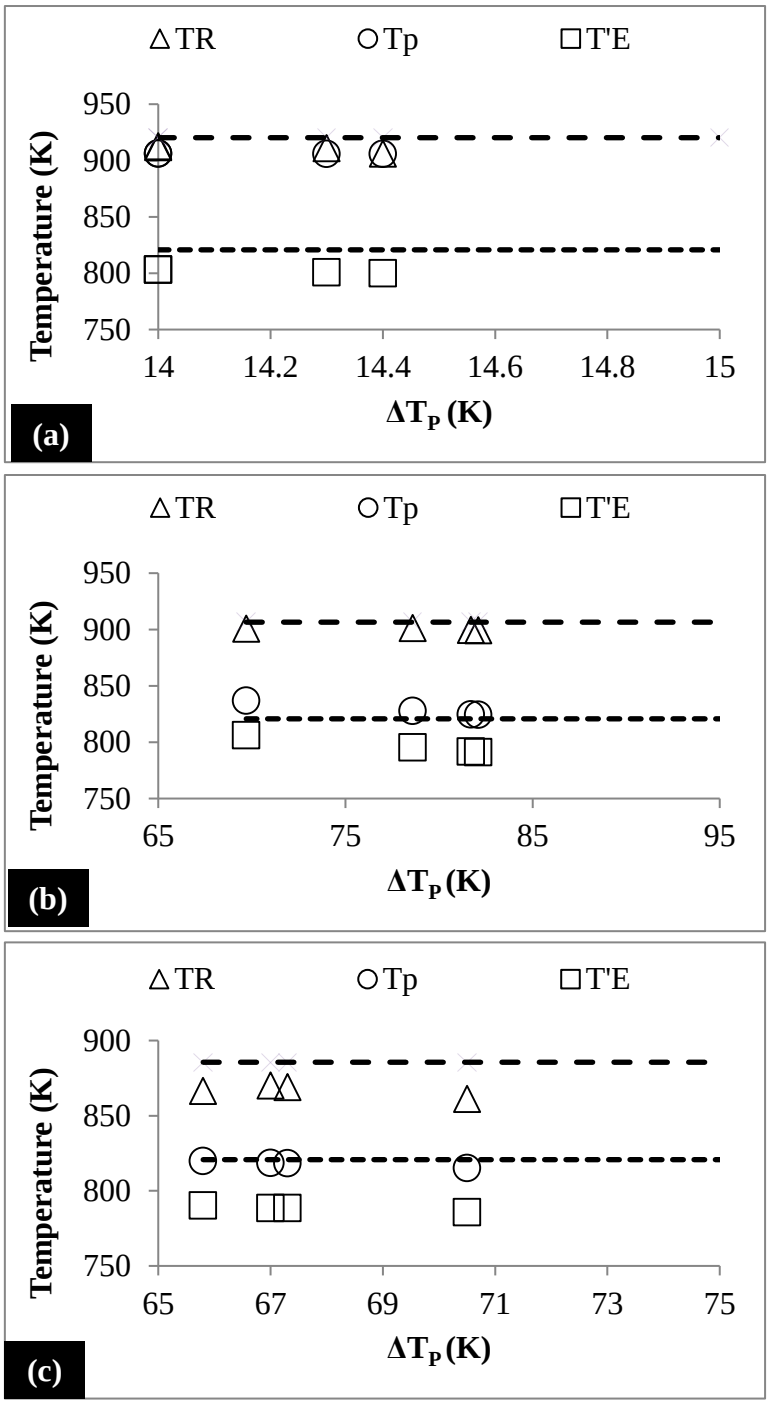

<u>Fig.10</u>: Characteristic temperatures during solidification as a function of primary dendritic nucleation undercooling ΔT_P (a) Al-5wt% Cu (b) Al-10wt% Cu (c) Al-17wt% Cu

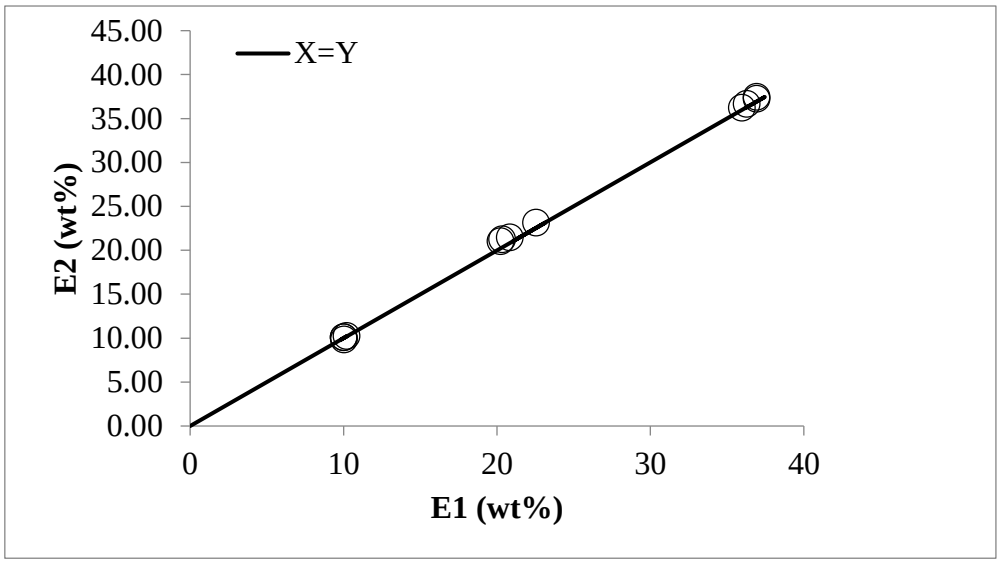

Fig.11: Comparison of model outputs of weight percent eutectic (E1) considering the primary dendritic nucleation undercooling and (E2) ignoring the primary dendritic nucleation undercooling.

List of tables

Table I: Impulse Atomized Al-Cu droplets of different compositions and sizes solidified in nitrogen and helium from melt at a temperature of 1123 K (850°C) [10]

Alloy Composition	Atomization gas	Droplet average size (μm)	F_E_Lever rule (LR) (wt.%)	F_E_Gulliver-Scheil (GS) (wt.%)
Al-5wt% Cu	He	196	0	12
		925		
	N_2	196		
		925		
Al-10wt% Cu	He	196	15	25
		925		
	N_2	234		
		925		
Al-17wt% Cu	He	196	41	46
		925		
	N_2	234		
		780		

Table II: Summary of the experimental results obtained by stereology and neutron diffraction[10] that lead to the estimation of eutectic fractions.

Alloy composition	Atomization Gas	Droplet size (μm)	Secondary Dendrite Arm Spacing (μm)	θ-Al_2Cu (w^{θ}) (wt.%)	F_E (wt.%)
Al-5wt% Cu	He	196	2.11	4.45	7.53
		925	5.63	4.55	7.62
	N_2	196	4.21	4.73	7.92
		925	7.07	4.71	7.88
Al-10wt% Cu	He	196	2.21	9.3	15.6
		925	4.62	9.2	15.4
	N_2	234	3.56	11.8	19.8
		925	5.93	9.98	16.7
Al-17wt% Cu	He	196	1.41	17.5	29.3
		925	3.16	18.13	31.7
	N_2	234	2.49	18.43	30.9
		780	4.46	18.45	30.9

Table III. Summary of the data used for the three investigated Al-Cu alloys

Parameter	Al-5wt.% Cu				Al-10wt.% Cu				Al-17wt.% Cu				Reference
	Size in µm (gas type)				Size in µm (gas type)				Size in µm (gas type)				
	196 (He)	925 (He)	196 (N_2)	925 (N_2)	196 (He)	925 (He)	234 (N_2)	925 (N_2)	196 (He)	925 (He)	234 (N_2)	780 (N_2)	
$\dot{T}$ *(K/s)*	4689	349	973	153	3546	258	608	113	2258	176	433	97	[10]
$\lambda_2 \times 10^{-6}$ *(m)*	2.11	5.63	4.21	7.07	2.21	4.62	3.56	5.93	1.41	3.16	2.49	4.46	[10]
k	0.22	0.22	0.22	0.22	0.28	0.28	0.21	0.26	0.31	0.28	0.29	0.28	[12]
C_E *(wt.% Cu)*	37.26	37.09	36.59	36.65	38.51	38.59	36.10	37.93	39.59	38.74	39.03	39.03	[12]
T_L	920.28				906.51				885.56				[12]
T_E	820.73				820.73				820.73				[12]
$A \times 10^{-6}$ *(m(K/s)^n)*	43.96				22.66				20.92				
n	0.35				0.28				0.35				
Γ *(K m)*	2.41×10^{-7}				2.41×10^{-7}				2.41×10^{-7}				[10]
D^l *(m^2s^{-1})*	1.05×10^{-7} exp(-2860/T)				1.05×10^{-7} exp(-2860/T)				1.05×10^{-7} exp(-2860/T)				[17]
m (K (wt.%)$^{-1}$)	-3.66				-3.86				-4.23				[10]
C_p^l *($J.m^{-3}.k^{-1}$)*	3.25×10^6				3.31×10^6				3.40×10^6				[17]
ΔH_f ($J.m^{-3}$)	1.09×10^9				1.13×10^9				1.18×10^9				[17]
ΔT_{hyp}	335				340				348				[17]

Table IV: Dendritic nucleation undercooling results based on the use of coarsening model [13] and eutectic nucleation undercooling estimated based on weight percent eutectic.

Alloy composition	Atomization Gas	Droplet size (µm)	F_E metastable phase diagram (wt.%)	Eutectic nucleation undercooling (K) (same in °C)	Dendritic nucleation undercooling (K) (same in °C)
Al-5wt% Cu	He	196	7.53	20.9	14.4
		925	7.62	20.0	14.3
	N_2	196	7.92	17.3	14.0
		925	7.88	17.6	14.0
Al-10wt% Cu	He	196	15.6	29.0	81.7
		925	15.4	29.5	82.1
	N_2	234	19.8	14.6	69.7
		925	16.7	25.4	78.6
Al-17wt% Cu	He	196	29.3	34.9	70.5
		925	31.7	30.4	65.8
	N_2	234	30.9	32.3	67.3
		780	30.9	32.2	67